Anisotropic Quantum Well Electro-Optics in Few-Layer Black Phosphorus

Michelle C. Sherrott,[†,‡,#] William S. Whitney,[§,#] Deep Jariwala,[†,‡,○] Souvik Biswas,[†] Cora M. Went,[‡,§] Joeson Wong,[†] George R. Rossman,[⊥,∥] and Harry A. Atwater*[,†,‡,⊥]

[†]Thomas J. Watson Laboratory of Applied Physics, California Institute of Technology, Pasadena, California 91125, United States
[‡]Resnick Sustainability Institute, California Institute of Technology, Pasadena, California 91125, United States
[§]Department of Physics, California Institute of Technology, Pasadena, California 91125, United States
[∥]Division of Geological and Planetary Sciences, California Institute of Technology, Pasadena, California 91125, United States
[⊥]Joint Center for Artificial Photosynthesis, California Institute of Technology, Pasadena, California 91125, United States

S *Supporting Information*

ABSTRACT: The incorporation of electrically tunable materials into photonic structures such as waveguides and metasurfaces enables dynamic, electrical control of light propagation at the nanoscale. Few-layer black phosphorus is a promising material for these applications due to its in-plane anisotropic, quantum well band structure, with a direct band gap that can be tuned from 0.3 to 2 eV with a number of layers and subbands that manifest as additional optical transitions across a wide range of energies. In this Letter, we report an experimental investigation of three different, anisotropic electro-optic mechanisms that allow electrical control of the complex refractive index in few-layer black phosphorus from the mid-infrared to the visible: Pauli-blocking of intersubband optical transitions (the Burstein–Moss effect); the quantum-confined Stark effect; and the modification of quantum well selection rules by a symmetry-breaking, applied electric field. These effects generate near-unity tuning of the BP oscillator strength for some material thicknesses and photon energies, along a single in-plane crystal axis, transforming absorption from highly anisotropic to nearly isotropic. Lastly, the anisotropy of these electro-optical phenomena results in dynamic control of linear dichroism and birefringence, a promising concept for active control of the complex polarization state of light, or propagation direction of surface waves.

KEYWORDS: Electro-optic tunability, black phosphorus, broadband, anisotropy, van der Waals materials
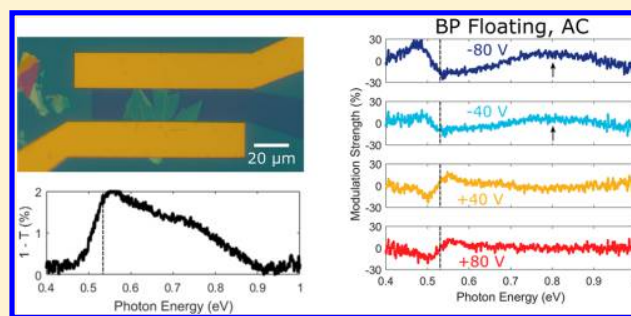
Dynamic control of the near- and far-field propagation of light is critical for next-generation optoelectronic devices. Ultrathin, layered materials are promising building blocks for this functionality, as they are easily incorporated into atom-scale structures, and their optical properties can be changed dramatically under applied electric fields.[1,2] Few-layer black phosphorus (BP) is particularly compelling due to its high electronic mobility, in-plane anisotropy, and thickness-tunable quantum well band structure, with a direct band gap that varies from 0.3 eV in bulk to 2 eV for monolayers.[3,4] Recent work using electrostatic gating and potassium ions has further shown that the electronic band gap of BP may be tuned by an electric field.[5−8] These unique attributes have already enabled the realization of novel and high-performance optoelectronic devices, including waveguide-integrated photodetectors.[9−13]

One of the most unusual features of BP is its large in-plane structural anisotropy, which generates to a polarization-dependent optical response[14−16] as well as mechanical,[17] thermal,[18] and electrical transport characteristics[19,20] that vary with in-plane crystallographic orientation.[21] This optical anisotropy corresponds to a large, broadband birefringence,[22] wherein the distinct optical index of refraction along each axis leads to a phase delay between polarization states of light. Moreover, mirror symmetry in the $x−z$ plane forbids intersubband optical transitions along the zigzag axis, and as a result, BP exhibits significant linear dichroism, wherein the material absorption depends strongly on the polarization state of exciting light.[15,23] An additional constraint on optical absorption corresponds to the naturally occurring quantum well nature of the BP band structure, wherein optical transitions are only allowed between subbands of opposite parities, because photons carry parity −1. For low-energy transitions, this corresponds to transitions between bands of equal quantum numbers (i.e., v_1 to c_1, v_2 to c_2), described in depth in ref 19.
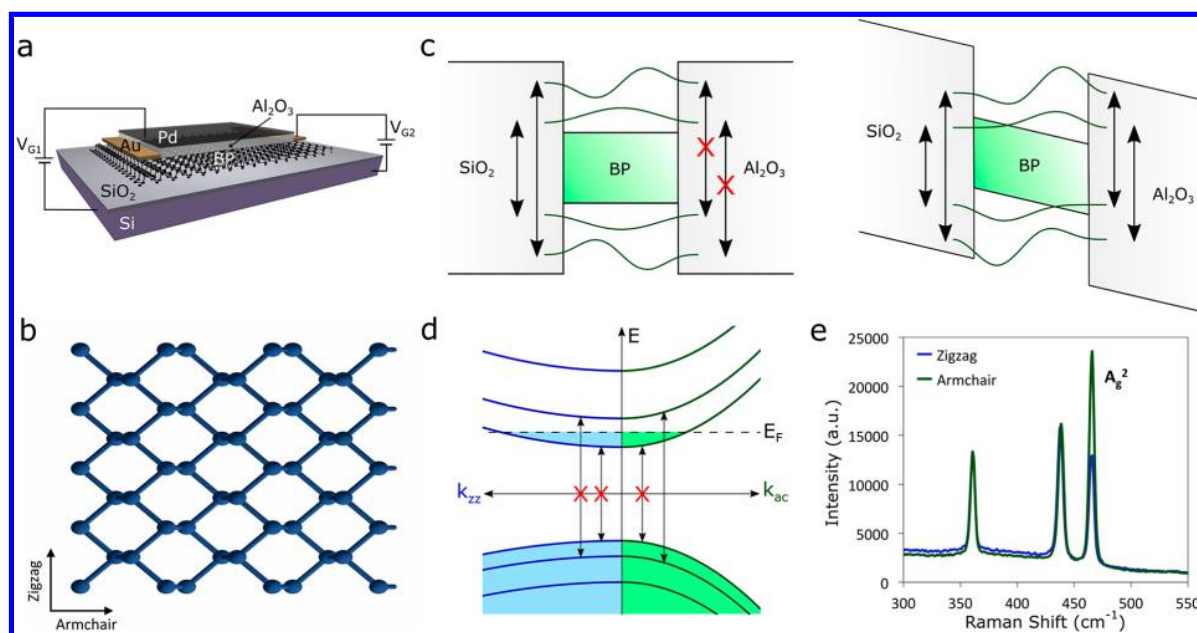
Figure 1. Anisotropic electro-optical effects in few-layer BP. (a) Schematic figure of infrared tunability devices. Few-layer BP is mechanically exfoliated on 285 nm SiO_2/Si and then capped with 45 nm Al_2O_3 by ALD. A semitransparent top contact of 5 nm Pd is used to apply a field (V_{G1}) while the device floats and 20 nm Ni/200 nm Au contacts are used to gate (V_{G2}) the contacted device. (b) Crystal structure of BP with armchair (AC) and zigzag (ZZ) axes indicated. (c) Illustration of two field-driven electro-optical effects: the quantum-confined Stark effect and symmetry-breaking modification of quantum well selection rules. In the quantum-confined Stark effect, an external field tilts the quantum well energy levels, causing a red-shifting of the intersubband transition energies. In the observed modification of selection rules, this field breaks the symmetry of the quantum well and orthogonality of its wave functions, allowing previously forbidden transitions to occur (e.g., from v_1 to c_2, a previously disallowed transition). (d) Illustration of anisotropic Pauli-blocking (Burstein−Moss effect) in BP. Intersubband transitions are blocked due to the filling of the conduction band. Along the ZZ axis, all optical transitions are disallowed regardless of carrier concentration. (e) Raman spectra with excitation laser polarized along AC and ZZ axes. The intensity ratio between the A_g^2 peak and the A_g^1 peak is used to identify crystal axes.

In this Letter, we use multiple field-effect device configurations to isolate and characterize three distinct, anisotropic electro-optic effects that allow significant control of the complex refractive index in BP. These effects are Pauli-blocking of intersubband optical transitions, also known as a Burstein−Moss or band-filling effect; the quantum-confined Stark effect; and modification of quantum well selection rules by a symmetry-breaking electric field. The resulting response approaches near-unity tunability of the BP oscillator strength for some BP thicknesses and photon energies. Further, this tuning is only along one in-plane crystal axis (the armchair direction). As a result, we are able to electrically control dichroism and birefringence in BP. In some cases, we observe tuning of the black phosphorus optical response from highly anisotropic to nearly isotropic. We observe this anisotropic tunability from the visible to mid-infrared (mid-IR) spectral regimes, behavior not seen in traditional electro-optic materials such as graphene,[24] transparent conducting oxides,[25,26] silicon,[27] and quantum wells.[28] This opens up the possibility of realizing novel photonic structures, in which linear dichroism in the van der Waals plane can be continuously tuned with low power consumption because the switching is electrostatic in nature. By controlling optical losses in the propagation plane, for example, efficient in-plane beam steering of surface plasmon polaritons or other guided modes is enabled. Moreover, an electrically tunable polarizer could be realized by modulating the polarization state of light absorbed in a resonant structure containing BP. Because this tunability is strongest at infrared wavelengths, it could also enable control of the polarization state of thermal radiation.[29−31]

In order to probe and distinguish the electro-optical tuning mechanisms evident in few-layer BP, we used a combination of gating schemes wherein the BP either floats electrically in an applied field or is contacted, as shown in Figure 1a and described further in the Methods section. We note that, for all experiments, the samples are exfoliated on an oxide surface and encapsulated in Al_2O_3; therefore, while strain effects are known to influence the band gap of 2D materials,[32−34] including few-layer BP, these are identical for all measurements. Polarization-dependent optical measurements are taken aligned to the crystal axes, in order to probe the structural anisotropy shown in Figure 1b. This enables us to isolate the contribution of charge-carrier density effects, i.e., a Burstein−Moss shift, and external field effects, i.e., the quantum-confined Stark effect and control of forbidden transitions in the infrared, to the tunability of linear dichroism, qualitatively illustrated in Figure 1c,d.[35−38] In the anisotropic Burstein−Moss (BM) shift, the optical band gap of the material is changed as a result of band-filling and the consequent Pauli-blocking of intersubband transitions. As the carrier concentration of the sample is changed, the Fermi level moves into (out of) the conduction or valence band, resulting in a decrease (increase) of absorptivity due to the disallowing (allowing) of optical transitions.[39,40] Because intersubband optical transitions are only allowed along the armchair axis of BP,[15,21,41] this tunability occurs only for light polarized along this axis. In the quantum-confined Stark Effect, the presence of a strong electric field results in the leaking of electron and hole wave functions into the band gap as Airy functions, red-shifting the intersubband transitions energies.[42] In quantum well struc-
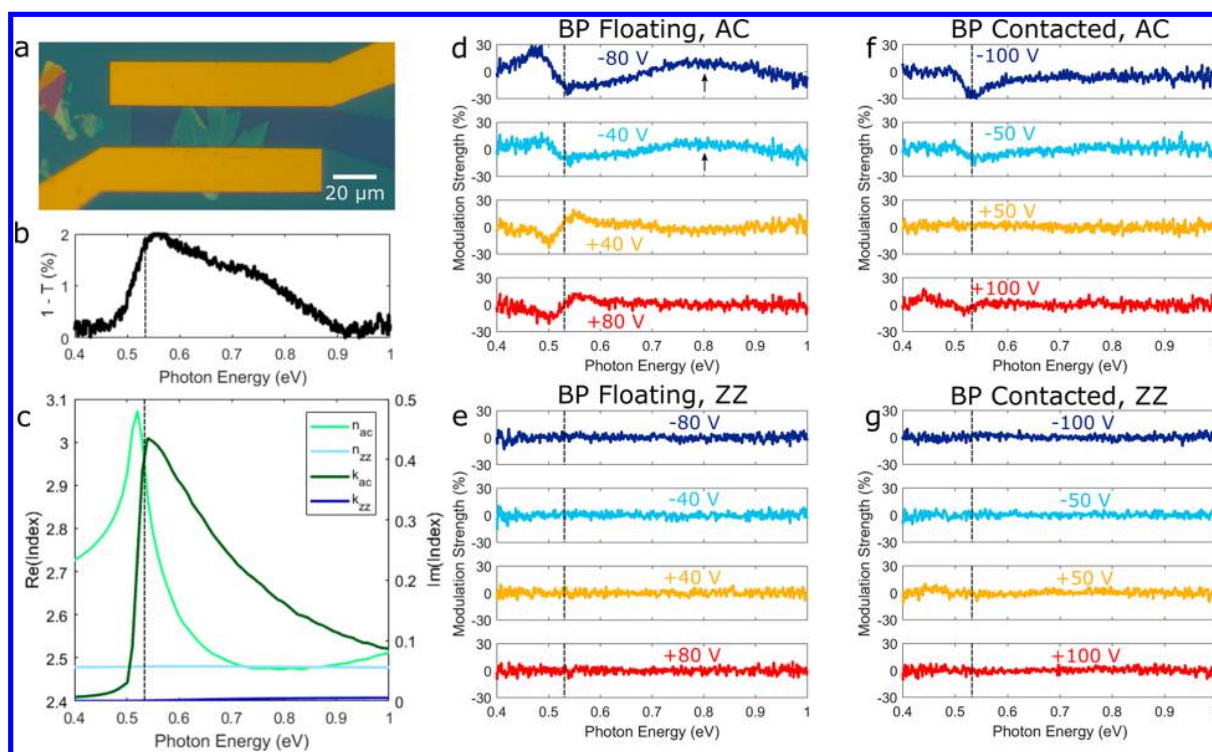
Figure 2. Electrically tunable linear dichroism: quantum-confined Stark and Burstein−Moss effects and forbidden transitions. (a) Optical image of a fabricated sample with two Au contact pads for direct electrical contact to the BP and a semitransparent Pd top contact between them, separated from the BP by a thin layer of Al$_2$O$_3$, as in the schematic of Figure 1a. (b) Zero-bias infrared extinction of 3.5 nm flake, polarized along the armchair (AC) axis. (c) Calculated index of refraction for 3.5 nm thick BP with a Fermi energy at the midgap. (d) Tunability of BP oscillator strength with a field applied to the floating device, for light polarized along the AC axis. (e) Corresponding tunability for light polarized along the zigzag (ZZ) axis. (f) Tunability of BP oscillator strength with gating of the contacted device, for light polarized along the AC axis. (g) Corresponding tunability for light polarized along the ZZ axis.

tures, this red-shifting is manifested for multiple subbands and therefore can be observed over a wide range of energies above the band gap. To assess the gate-tunable anisotropy of the optical response of BP, the armchair and zigzag axes, illustrated in Figure 1b, of the samples considered are identified by a combination of cross-polarized visible microscopy, described in the Supporting Information, and either polarization-dependent Raman spectroscopy or infrared measurements. We perform polarization-dependent Raman spectroscopy with the 532 nm excitation laser polarized parallel to one of the two crystal axes as determined by cross-polarized visible microscopy. The armchair and zigzag axes cannot be distinguished from the intensity of any of the Raman peaks alone, as the polarization behavior of each peak depends strongly on the excitation wavelength and the flake thickness.[43] However, for 532 nm excitation and all thicknesses, the ratio of the intensities of the A^{2}g and the A^{1}g Raman peaks is higher for the armchair than the zigzag axis, so this ratio remains a robust way to distinguish between the axes.[43,44] Representative Raman spectra are presented for the visible frequency sample on SrTiO$_3$ in Figure 1e.

To illustrate the mechanisms of tunable dichroism of BP in the mid-infrared, we measure tunability of transmittance using Fourier-transform infrared (FTIR) microscopy as a function of externally (V$_{G1}$) or directly applied bias (V$_{G2}$), presented for a 3.5 nm thick flake, as determined from atomic force microscopy (AFM) (Figure S1), in Figure 2. Figure 2b presents the raw extinction of the flake along the armchair axis at zero bias, obtained by normalizing the armchair axis

extinction to that of the optically inactive zigzag axis. A band edge of approximately 0.53 eV is measured, consistent with a thickness of 3.5 nm. A broad, weak shoulder feature is observed at approximately 0.75 eV. The corresponding calculated optical constants for the flake are presented in Figure 2c for comparison. A Kubo formula approach is used for this calculation, as is described in further detail under Calculations in the Methods section, and in refs 35−37.

Figure 2d,e illustrates the influence of an external field on the extinction of BP with carrier concentration held constant (i.e., the BP is left floating). The extinction data for each voltage is normalized to the zero-bias case and to the peak BP extinction seen in Figure 2b to obtain a tuning strength percentage that quantifies the observed tunability of the BP oscillator strength. In total, this tuning strength percentage at voltage V′ is defined as follows:

$$\text{modulation strength (\%)} = 100 \times \frac{-\Delta T_{V'/0V}\,(\%)}{\max(-\Delta T_{AC/ZZ})\,(\%)} \tag{1}$$

$$\text{where } -\Delta T_{A/B}\,(\%) = 100 \times \left(1 - \frac{T_A}{T_B}\right)$$

As an example, for the device examined in Figure 2, the maximum value of $-\Delta T_{AC/ZZ}$ is shown in Figure 2b to be approximately 2%. At its strongest, $-\Delta T_{V'/0V}$ approaches (for −80 V applied and a photon energy of 0.475 eV) about one-third of this 2% maximal BP extinction value, yielding a
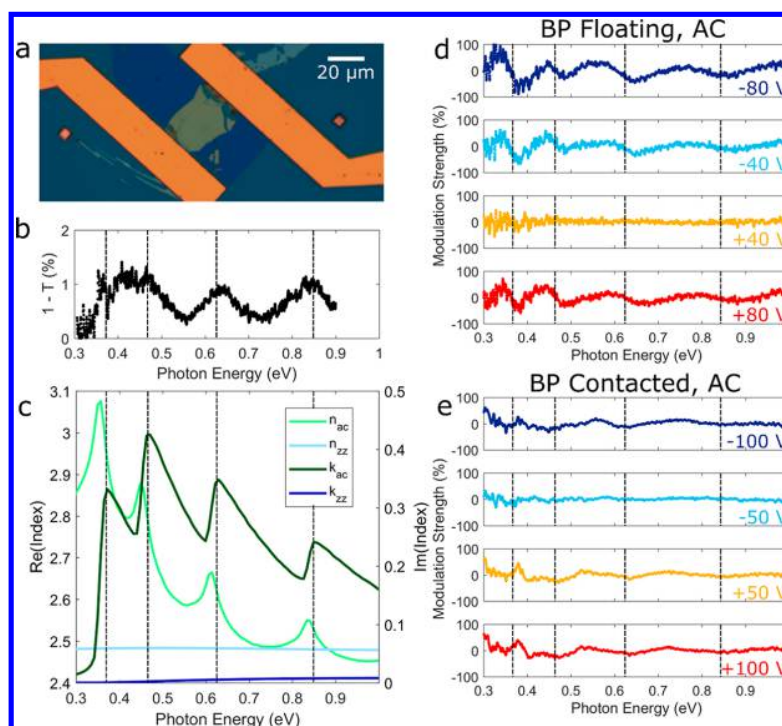
Figure 3. Variation of tunability with BP thickness. (a) Optical image of the fabricated 8.5 nm sample. (b) Zero-bias extinction of an 8.5 nm flake, polarized along the AC axis. (c) Calculated index of refraction for 8.5 nm thick BP. (d) Tuning of BP oscillator strength with a field applied to the floating device, for light polarized along the AC axis. (e) Tuning of BP oscillator strength with gating of the contacted device, for light polarized along the AC axis.

modulation strength of 30%. We note that this normalization scheme underestimates the tuning strength for photon energies where overall BP extinction is lower, such as away from any subband edges. Along the armchair axis, presented in Figure 2d, two tunable features are measured near photon energies of 0.5 and 0.8 eV. We explain the first feature at 0.5 eV as arising from a shifting of the BP band edge due to the quantum-confined Stark effect. At negative bias, the band gap effectively shrinks and this manifests as a redistribution of oscillator strength near the band edge to lower energies. As a result, an increase in absorptance is measured below the zero-bias optical band gap, and a decrease is seen above it. At positive bias, this trend is weakened and reversed. We propose two explanations for this asymmetry: the first is the influence of electrical hysteresis, and the second is the presence of a small internal field in the BP at zero bias, which has been observed in previous works on the infrared optical response of few-layer BP.[15]

The second, higher energy feature observed in the measured spectrum does not correspond to any predicted intersubband transition. Rather, we propose it arises due to the modification of quantum well selection rules that limit the allowed intersubband optical transitions in black phosphorus by the applied electric field. In a symmetric quantum well, only transitions between states with equal quantum numbers are allowed, as other states have orthogonal wave functions with zero overlap integrals.[36] However, a strong applied field breaks the symmetry of the quantum well and the orthogonality of its wave functions, eliminating this selection rule. We can likely assign this new feature to the first hybrid transition, E_{12}, consistent with literature results for a flake of the same thickness (6-layers) and zero-bias band gap energy.[15] Due to

some uncertainty in flake thickness, this feature could also be well-explained by a combination of the first two hybrid transitions for a 7-layer sample. We note that this feature is present in the 0 V extinction spectrum, consistent with a zero-bias internal field. As the symmetry is further broken with an externally applied electric field, this transition is strengthened. Under positive bias, the internal and external fields are in competition, resulting in minimal change. This suppressed tunability can also be attributed to hysteresis, as before.

In Figure 2e, no tunability is measured for any applied bias for light polarized along the zigzag axis. This can be well understood due to the dependence of the Stark effect on the initial oscillator strength of an optical transition; because no intersubband optical transitions are allowed along this axis, the field effect is weak. Similar behavior has been observed in excitons in ReS$_2$ based on an optical Stark effect.[45] Moreover, while the externally applied field can allow "forbidden" transitions along the armchair axis by breaking the out-of-plane symmetry of the quantum well, in-plane symmetry properties and thus the selection rule precluding all zigzag axis intersubband transitions are unaffected. This selection rule and the corresponding symmetry properties have been previously described.[19]

In Figure 2f,g, we present the complementary data set of tunable dichroism measurements due to a directly applied gate bias with electrical contact made to the BP in a standard field-effect transistor (FET) geometry. Here, we observe tunability dominated by carrier concentration effects. At the band gap energy of approximately 0.53 eV, a simple decrease in absorptance is observed at negative and large positive biases, consistent with an ambipolar BM shift. Unlike the results of applying field while the BP floats, no tunability of the
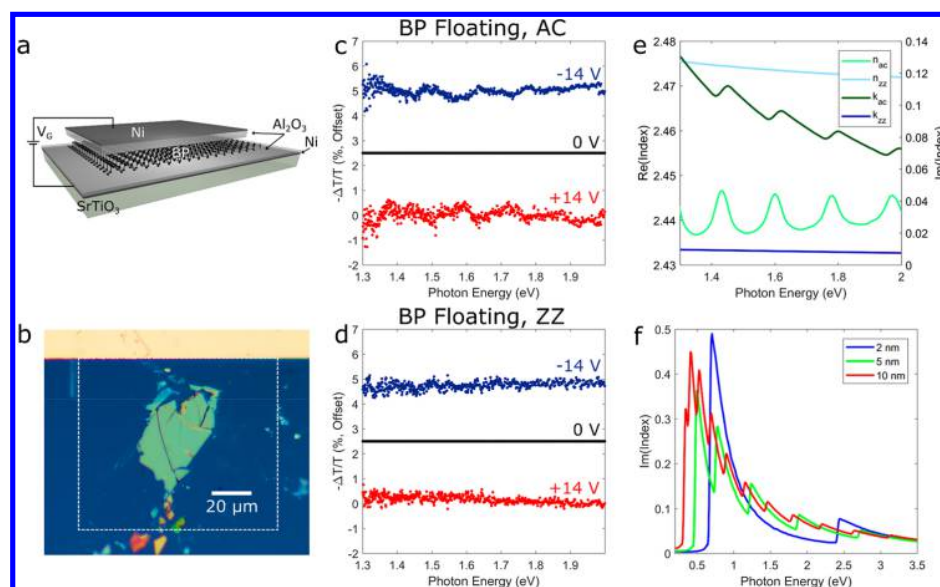
Figure 4. Tunability in the visible. (a) Schematic figure of the visible tuning device. Few-layer BP is mechanically exfoliated on 45 nm Al_2O_3/5 nm Ni on $SrTiO_3$ and then coated with 45 nm Al_2O_3. A 5 nm thick semitransparent Ni top contact is used. (b) Optical image of the fabricated sample with 20 nm thick BP. Dashed white line indicates the boundary of the top Ni contact. (c) Tuning of extinction with a field applied to the floating device, for light polarized along the AC axis. (d) Corresponding tuning for light polarized along the ZZ axis. (e) Calculated index of refraction for 20 nm thick BP for the measured energies. (f) Calculated imaginary index of refraction of several thicknesses of BP from the infrared to visible.

forbidden transition at 0.75 eV is observed; this is explained in part due to the screening of the electric field due to the carrier concentration tunability. We additionally may consider the possibility that this optical transition is disallowed by Pauli-blocking effects, negating the symmetry-breaking effect of the directly applied field. As in the case for the floating BP measurement, no tunability is observed along the zigzag axis.

The anisotropic electro-optical effects described above change character rapidly as the BP thickness, and hence band gap and band structure, is varied. Figure 3 presents analogous results on a flake of 8.5 nm thickness, determined by AFM (see Figure S1), for which an optical image is presented in Figure 3a. Due to the increased thickness, the energy separation between subbands is smaller, resulting in a narrower free-spectral range between absorptance features measured in the zero-bias spectrum, presented in Figure 3b and for which corresponding calculated optical constants are presented in Figure 3c. Results for tunability by an external field with the BP left floating are presented in Figure 3d. As in the thin flake, substantial tuning of the absorptance at each intersubband transition is observed due to the quantum-confined Stark effect (QCSE) red-shifting the energy of the subbands. Due to the large Stark coefficient in BP, which increases with thickness in the few-layer limit, absorption is nearly 100% suppressed, resulting in an approximately isotropic optical response from the material.[6,46] Unlike the previous sample, tuning of forbidden transitions is not apparent; all features correspond to transitions measured in the 0 V normalization scheme as well as the calculated optical constants for a thickness of 8.5 nm. As before, no tuning is seen along the zigzag axis, as shown in Figure S2. In Figure 3e, the tunability for directly gated, contacted BP is shown. The observed tuning, a reduction in extinction centered at each of the calculated intersubband transition energies, is relatively weak and does not persist to high photon energies. This suggests that the dominant tunability mechanism is the ambipolar BM shift, rather than

the QCSE. Additional measurements at lower energies are presented in Figure S3.

In Figure 4, we present results of gate-tunable dichroism at visible frequencies in a 20 nm thick flake. A new device geometry is used to enable transmission of visible light, shown schematically in Figure 4a and in an optical image in Figure 4b. In this configuration, a $SrTiO_3$ substrate is utilized to allow transmission-mode measurements at visible wavelengths. A symmetric gating scheme is devised based on semitransparent top and back gate electrodes of 5 nm Ni, as described in the Methods section. Only an applied field, floating BP measurement is utilized, as band-filling effects should be negligible at this energy range. In Figure 4c, we present tunability results from 1.3 to 2 eV. Due to the QCSE, tunability is observed up to 1.8 eV, corresponding to red light. Thus, we demonstrate that electro-optic tuning of linear dichroism is possible across an extraordinarily wide range of wavelengths in a single material system, enabling multifunctional photonic devices with broadband operation.

The decay of BP intersubband oscillator strength at higher photon energies provides a spectral cutoff for QCSE-based tunability, but for 5 nm BP or thinner, this oscillator strength is strong through the entire visible regime, as illustrated in Figure 4f. We thus suggest that, in very thin BP, strong tuning of absorption and dichroism is possible to even higher energies. By selecting a flake of 2 nm, for example, tunable linear dichroism is possible up to 3 eV from the band gap energy of 0.75 eV. A higher density of features, beginning at lower energies, may be introduced by utilizing a thicker flake, with a slightly decreased tuning strength, as seen for 5 and 10 nm thickness flakes. We also note that by substituting graphene top and bottom contacts or utilizing nanophotonic techniques to focus light in the BP, higher absolute tuning strength could be easily realized.

This phenomenon is in stark contrast to the gate-tunability of the optical responon of other 2D materials, where substantial

tunability is typically constrained to the narrowband energy of the primary exciton, as in MoS_2 and WS_2.[1,47] In another van der Waals materials system, monolayer graphene, tunability is accessible over a broader wavelength range due to the Pauli-blocking of optical transitions at $2E_F$; however, this is limited to the range over which electrostatic gating is effective, typically between $E_F \sim 0$ to $E_F \sim 0.5$ eV.[2,48] Moreover, these materials are not dichroic or birefringent in-plane, and so BP offers a novel phenomenon that can be taken advantage of to realize previously challenging or impossible photonic devices. The same restriction is true of bulk tunable materials such as quantum wells, transparent conducting oxides, and transition metal nitrides.

In summary, we have observed and isolated three competing, anistropic electro-optical effects in few-layer black phosphorus: the Pauli-blocking of intersubband transitions (Burstein−Moss effect), the quantum-confined Stark effect, and the modification of quantum well selection rules by a symmetry-breaking electric field. These effects, which produce near-unity changes in the black phosphorus oscillator strength for some material thicknesses and photon energies, can be tuned to a broad range of frequencies, from the mid-infrared to the visible, by controlling the thickness and thus band structure of the black phosphorus. Further, these are strongly anisotropic electro-optical effects, and we thus observe them to allow electrical control of both linear dichroism and birefringence. We observe that absorption in BP can be tuned from anisotropic to nearly isotropic. We suggest that these phenomena and this material are a promising platform for controlling the in-plane propagation of surface or waveguide modes, as well as for polarization-switching, phase and amplitude control, and reconfigurable far-field metasurfaces. As with van der Waals materials as a whole, few-layer black phosphorus provides a route not only to an improved material platform for optoelectronics but also to new physics and the potential new technology paradigms that follow.

Methods. *Infrared Sample Preparation.* Samples for infrared measurements were fabricated by mechanically exfoliating few-layer BP onto 285 nm SiO_2/Si in a glovebox environment. Contacts of 20 nm Ni/200 nm Au were fabricated by electron beam lithography, electron beam evaporation, and liftoff. A top gate dielectric of 45 nm Al_2O_3 was deposited by atomic layer deposition (ALD) following the technique in ref 49, and a semitransparent top contact of 5 nm Ni was deposited by electron beam evaporation and liftoff. Measurements were performed in a Fourier-transform infrared spectrometer coupled to a microscope.

Visible Sample Preparation. Samples for visible measurements were fabricated by depositing a 5 nm thick semitransparent back contact of Ni, followed by 45 nm Al_2O_3 by ALD on a 0.5 mm thick $SrTiO_3$ substrate. Few-layer BP was then mechanically exfoliated, and electrical contacts were fabricated as above. Measurements are performed in a visible spectrometer. Nickel was selected as the optimum metallic contact through finite-difference time-domain (FDTD) simulations presented in Figure S4.

Calculations. Calculations of the optical constants of BP are based on the formalism developed in ref 36. Optical conductivity, σ, is calculated using the Kubo formula within an effective low-energy Hamiltonian for different thicknesses. The permittivity is calculated as $\varepsilon(\omega) = \varepsilon_\infty + i\sigma/\omega\delta$ where δ is the thickness of the BP, and the high-frequency permittivity, ε_∞, is taken from ref 41.

ASSOCIATED CONTENT

Ⓢ Supporting Information

The Supporting Information is available free of charge on the ACS Publications website at DOI: 10.1021/acs.nanolett.8b03876.

> Identification of crystal axes, AFM characterization, additional sample spectra, visible sample substrate simulations, high modulation strength sample spectra, and comparison to theory (PDF)

AUTHOR INFORMATION

Corresponding Author

*E-mail: haa@caltech.edu.

ORCID Ⓘ

Michelle C. Sherrott: 0000-0002-7503-9714
William S. Whitney: 0000-0001-5269-2967
Joeson Wong: 0000-0002-6304-7602
Harry A. Atwater: 0000-0001-9435-0201

Present Address

○D.J.: Department of Electrical and Systems Engineering, University of Pennsylvania, Philadelphia, PA 19104, USA.

Author Contributions

#M.C.S. and W.S.W contributed equally.

Notes

The authors declare no competing financial interest.

ACKNOWLEDGMENTS

REFERENCES

(1) Mak, K. F.; He, K.; Lee, C.; Lee, G. H.; Hone, J.; Heinz, T. F.; Shan, J. Tightly Bound Trions in Monolayer MoS_2. *Nat. Mater.* **2013**, *12*, 207−211.

(2) Fei, Z.; Rodin, A. S.; Andreev, G. O.; Bao, W.; McLeod, A. S.; Wagner, M.; Zhang, L. M.; Zhao, Z.; Thiemens, M.; Dominguez, G.; et al. Gate-Tuning of Graphene Plasmons Revealed by Infrared Nano-Imaging. *Nature* **2012**, *487*, 82−85.

(3) Li, L.; Yu, Y.; Ye, G. J.; Ge, Q.; Ou, X.; Wu, H.; Feng, D.; Chen, X. H.; Zhang, Y. Black Phosphorus Field-Effect Transistors. *Nat. Nanotechnol.* **2014**, *9*, 372−377.

(4) Ling, X.; Wang, H.; Huang, S.; Xia, F.; Dresselhaus, M. S. The Renaissance of Black Phosphorus. *Proc. Natl. Acad. Sci. U. S. A.* **2015**, *112*, 4523−4530.

(5) Kim, J.; Baik, S. S.; Ryu, S. H.; Sohn, Y.; Park, S.; Park, B.-G.; Denlinger, J.; Yi, Y.; Choi, H. J.; Kim, K. S. Observation of Tunable Band Gap and Anisotropic Dirac Semimetal State in Black Phosphorus. *Science* **2015**, *349*, 723−726.

(6) Liu, Y.; Qiu, Z.; Carvalho, A.; Bao, Y.; Xu, H.; Tan, S. J. R.; Liu, W.; Castro Neto, A. H.; Loh, K. P.; Lu, J. Gate-Tunable Giant Stark Effect in Few-Layer Black Phosphorus. *Nano Lett.* **2017**, *17*, 1970−1977.

(7) Deng, B.; Tran, V.; Xie, Y.; Jiang, H.; Li, C.; Guo, Q.; Wang, X.; Tian, H.; Koester, S. J.; Wang, H.; et al. Efficient Electrical Control of Thin-Film Black Phosphorus Bandgap. *Nat. Commun.* **2017**, *8*, 14474.

(8) Peng, R.; Khaliji, K.; Youngblood, N.; Grassi, R.; Low, T.; Li, M. Midinfrared Electro-Optic Modulation in Few-Layer Black Phosphorus. *Nano Lett.* **2017**, *17*, 6315−6320.

(9) Youngblood, N.; Chen, C.; Koester, S. J.; Li, M. Waveguide-Integrated Black Phosphorus Photodetector with High Responsivity and Low Dark Current. *Nat. Photonics* **2015**, *9*, 247−252.

(10) Wang, T.; Hu, S.; Chamlagain, B.; Hong, T.; Zhou, Z.; Weiss, S. M.; Xu, Y.-Q. Visualizing Light Scattering in Silicon Waveguides with Black Phosphorus Photodetectors. *Adv. Mater.* **2016**, *28*, 7162−7166.

(11) Chen, C.; Youngblood, N.; Li, M. Study of Black Phosphorus Anisotropy on Silicon Photonic Waveguide. *2015 Optoelectronics Global Conference (OGC)* **2015**, 1−3.

(12) Huang, M.; Wang, M.; Chen, C.; Ma, Z.; Li, X.; Han, J.; Wu, Y. Broadband Black-Phosphorus Photodetectors with High Responsivity. *Adv. Mater.* **2016**, *28* (18), 3481−3485.

(13) Chen, C.; Youngblood, N.; Peng, R.; Yoo, D.; Mohr, D. A.; Johnson, T. W.; Oh, S.-H.; Li, M. Three-Dimensional Integration of Black Phosphorus Photodetector with Silicon Photonics and Nanoplasmonics. *Nano Lett.* **2017**, *17*, 985−991.

(14) Wang, X.; Jones, A. M.; Seyler, K. L.; Tran, V.; Jia, Y.; Zhao, H.; Wang, H.; Yang, L.; Xu, X.; Xia, F. Highly Anisotropic and Robust Excitons in Monolayer Black Phosphorus. *Nat. Nanotechnol.* **2015**, *10*, 517−521.

(15) Zhang, G.; Huang, S.; Chaves, A.; Song, C.; Özçelik, V. O.; Low, T.; Yan, H. Infrared Fingerprints of Few-Layer Black Phosphorus. *Nat. Commun.* **2017**, *8*, 14071.

(16) Liu, Z.; Aydin, K. Localized Surface Plasmons in Nanostructured Monolayer Black Phosphorus. *Nano Lett.* **2016**, *16*, 3457−3462.

(17) Wei, Q.; Peng, X. Superior Mechanical Flexibility of Phosphorene and Few-Layer Black Phosphorus. *Appl. Phys. Lett.* **2014**, *104*, 251915.

(18) Luo, Z.; Maassen, J.; Deng, Y.; Du, Y.; Garrelts, R. P.; Lundstrom, M. S.; Ye, P. D.; Xu, X. Anisotropic In-Plane Thermal Conductivity Observed in Few-Layer Black Phosphorus. *Nat. Commun.* **2015**, *6*, 9572.

(19) Yuan, H.; Liu, X.; Afshinmanesh, F.; Li, W.; Xu, G.; Sun, J.; Lian, B.; Curto, A. G.; Ye, G.; Hikita, Y.; et al. Polarization-Sensitive Broadband Photodetector Using a Black Phosphorus Vertical p−n Junction. *Nat. Nanotechnol.* **2015**, *10*, 707−713.

(20) Liao, B.; Zhao, H.; Najafi, E.; Yan, X.; Tian, H.; Tice, J.; Minnich, A. J.; Wang, H.; Zewail, A. H. Spatial-Temporal Imaging of Anisotropic Photocarrier Dynamics in Black Phosphorus. *Nano Lett.* **2017**, *17*, 3675−3680.

(21) Xia, F.; Wang, H.; Jia, Y. Rediscovering Black Phosphorus as an Anisotropic Layered Material for Optoelectronics and Electronics. *Nat. Commun.* **2014**, *5*, 5458.

(22) Lan, S.; Rodrigues, S.; Kang, L.; Cai, W. Visualizing Optical Phase Anisotropy in Black Phosphorus. *ACS Photonics* **2016**, *3*, 1176−1181.

(23) Qiao, J.; Kong, X.; Hu, Z.-X.; Yang, F.; Ji, W. High-Mobility Transport Anisotropy and Linear Dichroism in Few-Layer Black Phosphorus. *Nat. Commun.* **2014**, *5*, 5475.

(24) Sherrott, M. C.; Hon, P. W. C.; Fountaine, K. T.; Garcia, J. C.; Ponti, S. M.; Brar, V. W.; Sweatlock, L. A.; Atwater, H. A. Experimental Demonstration of > 230° Phase Modulation in Gate-Tunable Graphene−Gold Reconfigurable Mid-Infrared Metasurfaces. *Nano Lett.* **2017**, *17*, 3027−3034.

(25) Park, J.; Kang, J.-H.; Kim, S. J.; Liu, X.; Brongersma, M. L. Dynamic Reflection Phase and Polarization Control in Metasurfaces. *Nano Lett.* **2017**, *17*, 407−413.

(26) Huang, Y.-W.; Lee, H. W. H.; Sokhoyan, R.; Pala, R. A.; Thyagarajan, K.; Han, S.; Tsai, D. P.; Atwater, H. A. Gate-Tunable Conducting Oxide Metasurfaces. *Nano Lett.* **2016**, *16*, 5319−5325.

(27) Xu, Q.; Schmidt, B.; Pradhan, S.; Lipson, M. Micrometre-Scale Silicon Electro-Optic Modulator. *Nature* **2005**, *435*, 325−327.

(28) Kuo, Y.-H.; Lee, Y. K.; Ge, Y.; Ren, S.; Roth, J. E.; Kamins, T. I.; Miller, D. A. B.; Harris, J. S. Strong Quantum-Confined Stark Effect in Germanium Quantum-Well Structures on Silicon. *Nature* **2005**, *437*, 1334−1336.

(29) Inoue, T.; Zoysa, M. D.; Asano, T.; Noda, S. Realization of Dynamic Thermal Emission Control. *Nat. Mater.* **2014**, *13*, 928−931.

(30) Coppens, Z. J.; Valentine, J. G. Spatial and Temporal Modulation of Thermal Emission. *Adv. Mater.* **2017**, *29*, 1701275.

(31) Brar, V. W.; Sherrott, M. C.; Jang, M. S.; Kim, S.; Kim, L.; Choi, M.; Sweatlock, L. A.; Atwater, H. A. Electronic Modulation of Infrared Radiation in Graphene Plasmonic Resonators. *Nat. Commun.* **2015**, *6*, 7032.

(32) Rodin, A. S.; Carvalho, A.; Castro Neto, A. H. Strain-Induced Gap Modification in Black Phosphorus. *Phys. Rev. Lett.* **2014**, *112*, 176801.

(33) Wang, X.; Tian, H.; Xie, W.; Shu, Y.; Mi, W.-T.; Ali Mohammad, M.; Xie, Q.-Y.; Yang, Y.; Xu, J.-B.; Ren, T.-L. Observation of a Giant Two-Dimensional Band-Piezoelectric Effect on Biaxial-Strained Graphene. *NPG Asia Mater.* **2015**, *7*, No. e154.

(34) Xu, K.; Wang, K.; Zhao, W.; Bao, W.; Liu, E.; Ren, Y.; Wang, M.; Fu, Y.; Zeng, J.; Li, Z.; et al. The Positive Piezoconductive Effect in Graphene. *Nat. Commun.* **2015**, *6*, 8119.

(35) Whitney, W. S.; Sherrott, M. C.; Jariwala, D.; Lin, W.-H.; Bechtel, H. A.; Rossman, G. R.; Atwater, H. A. Field Effect Optoelectronic Modulation of Quantum-Confined Carriers in Black Phosphorus. *Nano Lett.* **2017**, *17*, 78−84.

(36) Low, T.; Rodin, A. S.; Carvalho, A.; Jiang, Y.; Wang, H.; Xia, F.; Castro Neto, A. H. Tunable Optical Properties of Multilayer Black Phosphorus Thin Films. *Phys. Rev. B: Condens. Matter Mater. Phys.* **2014**, *90*, No. 075434.

(37) Lin, C.; Grassi, R.; Low, T.; Helmy, A. S. Multilayer Black Phosphorus as a Versatile Mid-Infrared Electro-Optic Material. *Nano Lett.* **2016**, *16*, 1683−1689.

(38) Deng, B.; Tran, V.; Xie, Y.; Jiang, H.; Li, C.; Guo, Q.; Wang, X.; Tian, H.; Koester, S. J.; Wang, H.; et al. Efficient Electrical Control of Thin-Film Black Phosphorus Bandgap. *Nat. Commun.* **2017**, *8*, 14474.

(39) Burstein, E. Anomalous Optical Absorption Limit in InSb. *Phys. Rev.* **1954**, *93*, 632−633.

(40) Moss, T. S. Theory of the Spectral Distribution of Recombination Radiation from InSb. *Proc. Phys. Soc., London, Sect. B* **1957**, *70*, 247.

(41) Wang, X.; Lan, S. Optical Properties of Black Phosphorus. *Adv. Opt. Photonics* **2016**, *8*, 618−655.

(42) Miller, D. A. B.; Chemla, D. S.; Damen, T. C.; Gossard, A. C.; Wiegmann, W.; Wood, T. H.; Burrus, C. A. Band-Edge Electroabsorption in Quantum Well Structures: The Quantum-Confined Stark Effect. *Phys. Rev. Lett.* **1984**, *53*, 2173−2176.

(43) Ling, X.; Huang, S.; Hasdeo, E. H.; Liang, L.; Parkin, W. M.; Tatsumi, Y.; Nugraha, A. R. T.; Puretzky, A. A.; Das, P. M.; Sumpter, B. G.; et al. Anisotropic Electron-Photon and Electron-Phonon Interactions in Black Phosphorus. *Nano Lett.* **2016**, *16*, 2260−2267.

(44) Hsiao, Y.; Chang, P.-Y.; Fan, K.-L.; Hsu, N.-C.; Lee, S.-C. Black Phosphorus with a Unique Rectangular Shape and Its Anisotropic Properties. *AIP Adv.* **2018**, *8*, 105216.

(45) Sim, S.; Lee, D.; Noh, M.; Cha, S.; Soh, C. H.; Sung, J. H.; Jo, M.-H.; Choi, H. Selectively Tunable Optical Stark Effect of Anisotropic Excitons in Atomically Thin ReS$_2$. *Nat. Commun.* **2016**, *7*, 13569.

(46) Dolui, K.; Quek, S. Y. Quantum-Confinement and Structural Anisotropy Result in Electrically-Tunable Dirac Cone in Few-Layer Black Phosphorous. *Sci. Rep.* **2015**, *5*, 11699.

(47) Chernikov, A.; van der Zande, A. M.; Hill, H. M.; Rigosi, A. F.; Velauthapillai, A.; Hone, J.; Heinz, T. F. Electrical Tuning of Exciton Binding Energies in Monolayer WS$_2$. *Phys. Rev. Lett.* **2015**, *115*, 126802.

(48) Brar, V. W.; Jang, M. S.; Sherrott, M.; Lopez, J. J.; Atwater, H. A. Highly Confined Tunable Mid-Infrared Plasmonics in Graphene Nanoresonators. *Nano Lett.* **2013**, *13*, 2541−2547.

(49) Wood, J. D.; Wells, S. A.; Jariwala, D.; Chen, K.-S.; Cho, E.; Sangwan, V. K.; Liu, X.; Lauhon, L. J.; Marks, T. J.; Hersam, M. C.

Effective Passivation of Exfoliated Black Phosphorus Transistors against Ambient Degradation. *Nano Lett.* **2014**, *14*, 6964−6970.